# Predictive Capability of MHD Stability Limits in High Performance DIII–D Discharges

A.D. Turnbull,[1] D. Brennan,[2] M.S. Chu,[1] L.L. Lao,[1] J.R. Ferron,[1] A.M. Garofalo,[3] P.B. Snyder,[1] J. Bialek,[3] I.N. Bogatu,[4] J.D. Callen,[5] M.S. Chance,[6] K. Comer,[5] D.H. Edgell,[4] S.A. Galkin,[7] D.A. Humphreys,[1] J.S. Kim,[4] R.J. La Haye,[1] T.C. Luce,[1] M. Okabayashi,[6] B.W.Rice,[8] E.J. Strait,[1] T.S. Taylor,[1] and H.R. Wilson[9]

[1]General Atomics, P.O. Box 85608, San Diego, California 92186-5608, USA
[2]Oak Ridge Institute for Science Education (presently at General Atomics)
[3]Columbia University (presently at General Atomics)
[4]FARTECH, P.O. Box 221053, San Diego, CA 92192, California, USA
[5]University of Wisconsin-Madison, Madison, Wisconsin 53706-3587, USA
[6]Princeton Plasma Physics Laboratory (presently at General Atomics)
[7]University of California-San Diego, La Jolla, California 92093-0319, USA
[8]Lawrence Livermore National Laboratory (present address: Xenogen, 860 Atlantic, Alameda, California 94501, USA
[9]Culham Laboratory, UKAEA, Abingdon, Oxfordshire OX14 3DB, UK

email: turnbull@fusion.gat.com

**Abstract**. Results from an array of theoretical and computational tools developed to treat the instabilities of most interest for high performance tokamak discharges are described. The theory and experimental diagnostic capabilities have now been developed to the point where detailed predictions can be productively tested so that competing effects can be isolated and either eliminated or confirmed. The predictions using high quality discharge equilibrium reconstructions are tested against the observations for the principal limiting phenomena in DIII–D: L–mode negative central shear (NCS) disruptions, H–mode NCS edge instabilities, and tearing and resistive wall modes (RWMs) in long pulse discharges. In the case of predominantly ideal MHD instabilities, agreement between the code predictions and experimentally observed stability limits and thresholds can now be obtained to within several percent, and the predicted fluctuations and growth rates to within the estimated experimental errors. Edge instabilities can be explained by a new model for edge localized modes as predominantly ideal low to intermediate n modes. Accurate ideal calculations are critical to demonstrating RWM stabilization by plasma rotation and the ideal eigenfunctions provide a good representation of the RWM structure when the rotation slows. Ideal eigenfunctions can then be used to predict stabilization using active feedback. For non-ideal modes, the agreement is approaching levels similar to that for the ideal comparisons; $\Delta'$ calculations, for example, indicate that some discharges are linearly unstable to classical tearing modes, consistent with the observed growth of islands in those discharges.

## 1. Introduction

Development of a fully predictive capability for the MHD stability limits in high performance tokamak discharges is critical to the success of the Advanced Tokamak program. This paper describes the recent results from an array of theoretical and computational tools that have been developed to treat the instabilities of most interest for high performance discharges. Ideal MHD provides accurate predictions for the highest achievable $\beta$ limits in tokamaks, and is now generally regarded as a reliable tool for predicting general trends. Ideal MHD can also be applied to make detailed predictions of mode structures and growth rates for specific discharges. Agreement between the code predictions and experimentally observed stability limits can now be obtained to within several percent in many cases, and the predicted fluctuations and growth rates to within the estimated experimental errors. Accurate reproduction of the equilibrium details, as well as experimental diagnostic details, is a key to obtaining this level of quantitative agreement. In particular, Motional Stark Effect (MSE) measurements of the local field line pitch across the plasma have been crucial. Non-ideal modes also limit tokamak performance and non-ideal effects are often important for explaining some of the details observed in the experiments. In this case, the stability is often even more sensitive to the equilibrium details. Nevertheless, the remaining discrepancies are being reduced by improved equilibrium reconstructions, and the agreement is approaching levels similar to that for the ideal comparisons.

The limiting phenomena in DIII–D can be categorized as follows. Discharges reaching the highest peak performance are generally limited in duration by fast growing instabilities; for L–mode edge high performance discharges, this is a disruptive toroidal mode number n=1 instability and for H–mode discharges, the high performance phase is usually terminated (without disruption) by an edge localized mode (ELM). On the other hand, performance in long pulse discharges is generally limited by the onset of slowly growing classical or neoclassical tearing modes (NTMs) triggered by a seed island by a sawtooth crash or ELM, or by resistive wall modes (RWMs), and these limit $\beta$ below the highest achievable peak values.

The theory and experimental diagnostic capabilities have now been developed to the point where detailed predictions can be productively tested so that the competing non-ideal effects can be isolated and either eliminated or confirmed. The predictions are tested against the observations for each of the limiting phenomena in DIII–D. For predominantly ideal plasma modes, the predicted modes are in good quantitative agreement with measured fluctuations from external Mirnov loops and internal electron cyclotron emission (ECE) diagnostics, providing direct identification of the observed instabilities. This knowledge can then be used to make experimental progress by controlling discharges to avoid or minimize the instabilities or, in the case of the RWM, by designing active stabilization systems. Tearing stability calculations are found to be significantly more sensitive to the details of the equilibrium reconstruction than for ideal stability. However, recent full 2D, finite $\beta$ stability calculations using accurately reconstructed equilibria for both a low $\beta$ discharge and a recent high performance discharge in DIII–D at several times show good agreement between the predicted $\Delta'$ and the observed onset of linearly unstable tearing modes.

## 2. Limits to Peak Performance

### 2.1. Global Kink Stability

In DIII–D and many other tokamaks, L–mode discharges with strong internal transport barriers and consequent highly peaked pressure profiles invariably disrupt [1] due to an n=1 instability at around $\beta_N \sim 2$. Here, $\beta_N$ is the usual normalized $\beta$, $\beta_N = \beta/(I/aB)$ (or Troyon coefficient) [2].The instability has many of the characteristics of an ideal mode. However, the observed growth of the mode in DIII–D of $\tau \sim 200\ \mu s$ is typically between the fast characteristic ideal instability time scale $\tau_I \sim 10\ \mu s$ and resistive plasma time scale $\tau_R \gtrsim 10$ ms [3,4].

A new model for the growth of an ideal instability, taking into account the effect of slowly passing through the instability boundary [5], resolves this issue. This model predicts that the subsequent mode growth is given by

$$\xi \sim \xi_0 \exp\left[(t/\tau)^{3/2}\right],$$

where $\tau = (2/3)^{2/3} \tau_{MHD}^{2/3} \tau_H^{1/3}$ with $\tau_{MHD}^{-1} \propto d\gamma^2/d\beta$ proportional to the ideal incremental growth rate, and $\tau_H^{-1}$ the characteristic heating rate — the rate at which $\beta$ increases. $\tau_{MHD}$ is of the same order as $\tau_I$ but for $\tau_H >> \tau_{MHD}$, $\tau$ is a hybrid between the $\tau_{MHD}$ time scale and the slower $\tau_H$ scale and then is much greater than $\tau_{MHD}$.

The new model fits the observed growth in the instantaneous amplitude of the Mirnov $\delta B(t)$ and soft x–ray (SXR) signals well, as shown in Fig. 1 for discharge #87009. From the known heating rate $\tau_H \simeq 1.5$ s and the best fit for $\tau$ in Fig. 1 of $\tau \sim 490\ \mu s$, one obtains an estimate of $\tau_{MHD} \simeq 9\ \mu s$. $\tau_{MHD}$ can also be found using a series of ideal stability calculations with increasing $\beta$ to obtain $\gamma(\beta)$. In principle, $\beta$ should be increased using the measured incremental pressure and current density profiles in the experiment. For the purpose of this comparison, however, the calculations used a sequence of equilibria in which the pressure profile functional form is held fixed and the current profile is adjusted to minimize the statistical $\chi^2$ fit to all the remaining data from the original equilibrium fit. This yields values of $\tau_{MHD} \sim 3\ \mu s$ to $5\ \mu s$, depending on the initial equilibrium chosen, which also provides a reasonable fit to the observed growth (Fig. 1).

This should be considered remarkable quantitative agreement given the approximately 20% uncertainty in the evaluation of the experimental value of $\tau_{MHD}$, the sensitivity of $\gamma$ to variations in the initial equilibrium reconstruction, and the arbitrariness of the choice of path in parameter space to obtain $\gamma(\beta)$. This appears to be the first quantitative comparison of a linear ideal growth rate prediction with a direct observation for a growing mode.

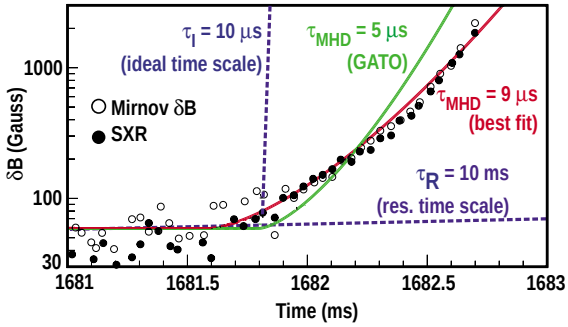


*Fig. 1. Time evolution of Mirnov and SXR signals during the disruption in discharge #87009 showing exp[(t/τ)$^{3/2}$] dependence.*

## 2.2. Edge stability

The highest peak performance in DIII–D is limited by edge instabilities [6]. Operationally these instabilities in NCS H–mode discharges appear as a large type I ELM after the initial high performance ELM-free period [7]. In contrast to normal type I ELMs, however, the high confinement is destroyed and rarely recovered as the discharge reverts to normal ELMing H–mode; the subsequent type I ELMs do not permanently reduce confinement further. An understanding of ELMs is essential to making further progress in extending these high performance discharges.

Experiments and closely coupled analysis for ELMing discharges in DIII–D have led to a new working model for ELMs [7,8] based on the idea that ELMs are edge localized, low to intermediate n ideal modes driven unstable by a combination of the large edge pressure gradient and its associated bootstrap current. The distinction between benign and large type I ELMs is determined in the context of this working model in terms of different radial penetration of the unstable kink mode into the core.

Verification of this model requires stability calculations for real diverted equilibria over the full range of toroidal mode numbers, including nonideal effects such as finite orbit stabilization at high n. Accurate reconstructions with particular attention to the profiles in the edge region are necessary as well. Equilibrium analysis tools, in which sharp pressure gradients and edge bootstrap-aligned current densities are modeled in order to better fit the discharge data, are now being included in the reconstructions. The global stability code GATO has been extended to accurately treat modes with n up to 10, and the ballooning phase factor extraction [9] is being extended to include free boundary modes. Also, the ELITE edge stability code [10], which uses the peeling-ballooning approximation valid for intermediate to high n, is now able to treat real equilibria instead of the previous local equilibrium model.

Figure 2 shows the results obtained so far with these new tools as applied to two series of equilibria with increasing edge pressure gradient $P'_{edge}$ and bootstrap aligned current in the pedestal region. The upper curve shows the $P'_{edge}$ limit for each n for equilibria based on a DIII–D discharge with moderate squareness, $\zeta$, which exhibited regular type I ELMs. Infinite n ballooning calculations show the large pressure gradient region at the edge has access to second stability in this case, consistent with the calculations from ELITE and GATO, and the calculations predict the most unstable mode with $n \gtrsim 10$. In contrast, for a series based on a high $\zeta$ discharge without second regime access that exhibited small frequent ELMs, the calculations show the most unstable n to be much higher — around the limit where finite orbit stabilization sets in. A comparison of the computed unstable modes for the two series shows that the instability in the case without second stability access is significantly less radially extended and according to the model would then result in smaller ELMs, as is observed. The calculations for these model equilibria also show reasonable quantitative agreement with the measured $P'_{edge}$ thresholds [8].

The n=5 mode calculated using the GATO code for a standard ELMing H–mode discharge (#92001) just prior to a type I ELM is shown in Fig. 3(a). This shows some radial extension but is fairly limited. The calculation was repeated for the first large type I ELM in a high

performance NCS mode is shown in Fig. 3(b). In both cases, a range of $n \gtrsim 3$ was found to be unstable and the radial penetration to the core decreases only weakly with increasing n. For discharge #87099, the mode penetrates well into the half radius. The computed mode widths correlate with the sizes of the observed ELM; in discharge #92001 the H–mode confinement was not permanently destroyed — the discharge continued as a standard ELMing H–mode, but for discharge #87099, the type I ELM destroyed the good internal confinement and the discharge reverted to ELMing H–mode.

### 3. Wall Stabilization

Wall stabilization of rotating DIII–D discharges was convincingly demonstrated in Refs. 11 and 12 by using comparisons of ideal stability limits with and without the DIII–D vacuum vessel modeled as a perfect conductor. Crucial to that demonstration were accurate equilibrium reconstructions using measured profiles and boundary and wall shapes [11], with sensitivity studies over allowed equilibrium variations consistent with the measured data. Also, when the rotation slowed, an instability with the characteristics of the expected RWM resulted in each case [11,12].

The first direct comparison of the predicted and measured RWM radial structure was also reported in Ref. 12. This comparison has since been refined and extended by choosing times with higher quality radial ECE profile data for the same discharge and by comparing the calculated poloidal mode structure with the Mirnov measured perturbed poloidal field. This is shown in Fig. 4. As in Ref. 12, the prediction from the GATO code is for an ideal mode with no wall, based on the assumption that for low mode rotation, the RWM is essentially the ideal kink slowed down to a wall growth time but otherwise little modified. The predicted and measured ECE radial profiles are in good agreement for two times corresponding to two different phases as the mode rotated past the ECE detectors. The arbitrary amplitude in the GATO prediction was adjusted here to fit the data at 1336.5 msec and scaled proportionally to the measured change in saddle loop signal for t=1332 msec. The phase at 1336.5 ms was chosen to obtain the best fit but constrained

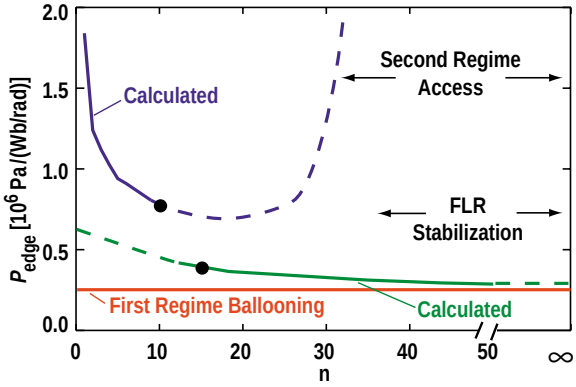


*Fig. 2. Calculated (solid curve) and inferred (dashed curve) $P'_{edge}$ thresholds versus n for a model DIII–D high ζ discharge (lower curve) and a moderate ζ discharge (upper curve).*

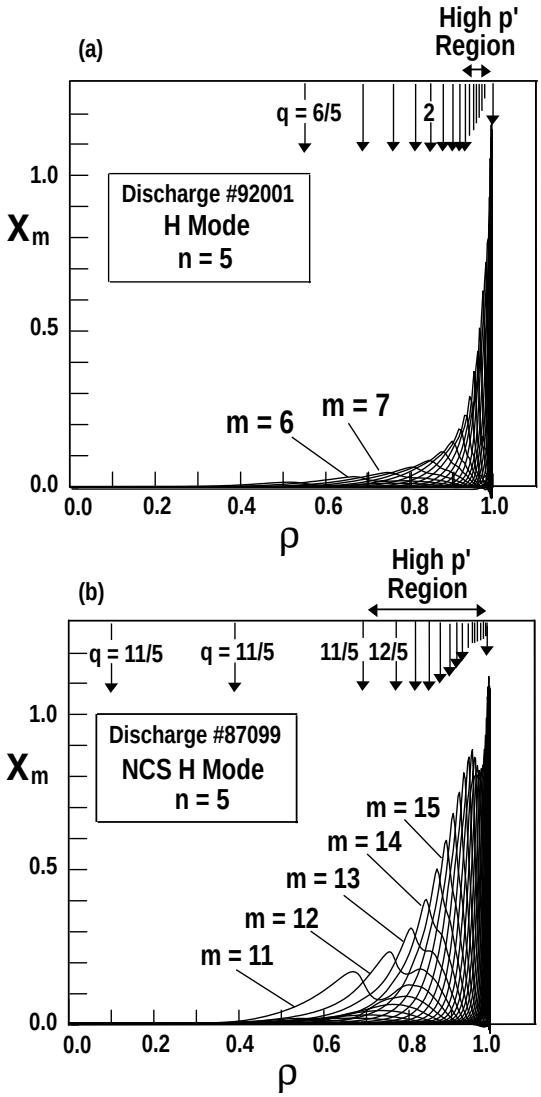


*Fig. 3. Computed n=5 eigenfunctions for equilibria reconstructed from (a) ELMing H–mode discharge #92001 and (b) high performance H–mode discharge #87099 immediately before the first ELM in each case.*

within the range that is consistent with the toroidal Mirnov array. The phase change between 1332 ms and 1336.5 ms from this array was then applied to the computed mode to obtain the prediction at 1332 ms. The agreement in magnitude, phase, and radial profile is extremely good.

The poloidal Mirnov fluctuations were also predicted and compared as shown in Fig. 4(b). The measured signal contains a significant axisymmetric component due to changes in the equilibrium during the growth of the RWM which must be extracted. In this case, a relatively primitive model for these changes corresponding to a uniform drop in current plus a rigid radial and vertical shift was used. Nevertheless, the prediction is good on the outboard side. There is some discrepancy on the inboard side where the mode has small amplitude and the data has large scatter, which can be accounted for by including a more sophisticated equilibrium shift model.

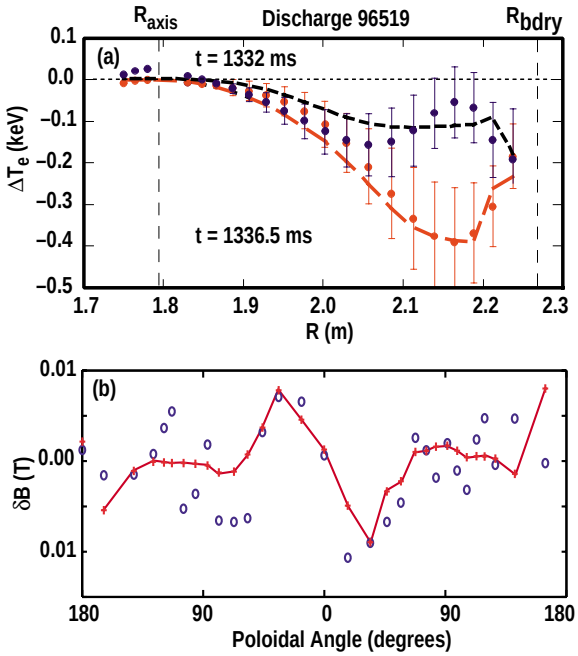


*Fig. 4. Predicted (a) radial ECE profile and (b) poloidal Mirnov signal for the RWM in discharge #96519 compared to measured diagnostic signals. The ECE profile in (a) shows two times with different toroidal phase.*

Active feedback stabilization of the RWM is an alternative to stabilization by plasma rotation. The calculations shown in Fig. 4 indicate that the ideal no-wall eigenfunction is a good representation of the RWM. The GATO ideal stability code has recently been coupled to the VACUUM codes [13] which includes the fields from active coils placed near the plasma. The coupled codes then self-consistently incorporate the coil response for a variety of feedback schemes to the plasma displacement and the corresponding response of the plasma to the vacuum fields induced by the active coils. Figure 5 shows the results from a design study for DIII–D using the coupled code [13]. Each curve corresponds to a fixed number of independent coils $n_f$ with a complete toroidal coverage, and the horizontal axis is the fraction of the poloidal circumference covered f — each coil thus spans a fraction $f/n_f$ of the poloidal circumference. The vertical axis shows the effectiveness $E_{ff}=(\delta W-\delta W^{no\,wall})/(\delta W^{ideal\,wall}-\delta W^{no\,wall})$ so that $E_{ff}=0$ corresponds to no wall and $E_{ff}=1$ to a perfectly conducting poloidally continuous wall at the coil location. The curves reveal two effects. First, the effectiveness increases with increased coverage for each $n_f$ up to a maximum, after which increased coverage degrades the effectiveness since then the mode scale length cannot be resolved by the finite coil spanning $f/n_f$. Thus there is an optimum coverage value $f_{opt}$ which increases with $n_f$. Second, the effectiveness $E_{ff}$ increases with $n_f$; this is true for fixed coverage as well as taking the optimum coverage $f_{opt}$ for each $n_f$.

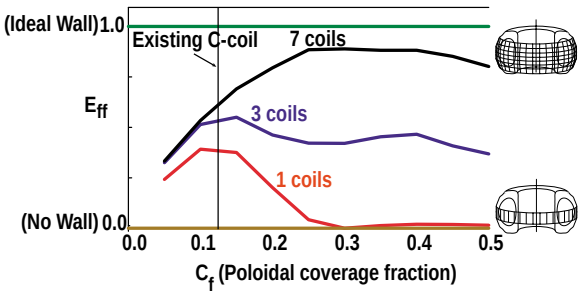


*Fig. 5. Calculated effectiveness $E_{ff}$ of feedback system versus poloidal coverage, $C_f$. $E_{ff}$ is normalized to an equivalent fully enclosing ideal wall at the coil location. The curves correspond to the poloidal coverage split into 1, 3, or 7 independent coils as indicated.*

The GATO code is also coupled to the VALEN code [14] which takes a fixed perturbation and computes the growth of this mode in the presence of a realistic 3D coil set such as the present error field correction C-coils on DIII–D. The GATO-VACUUM calculations described above demonstrate that the deformation of the RWM by the active coils was small for the

configuration studied. Thus, the fixed mode used in VALEN is a good model in this case. The GATO-VALEN calculations show that with the present C-coil configuration, consisting of six coils near the midplane and the present external flux loop sensors, the β limit in DIII–D could be increased into the wall stabilized β range by approximately 10% of the difference between the ideal wall and no wall limits ($\beta^{\text{ideal wall}}$-$\beta^{\text{no wall}}$). However, by adding six coils above and six coils below the current set and utilizing internal poloidal field sensors as well as external and internal flux loop sensors, this could be increased to 80%, thus approaching the β limit achievable with a perfectly conducting vacuum vessel. These results are now being incorporated into plans for enhancing the feedback system on DIII–D.

## 4. Tearing Mode Stability

Tearing modes often limit β in long pulse DIII–D discharges. These are frequently triggered by some other event such as a sawtooth, ELM, or more recently [15] a RWM, and are usually interpreted as neoclassical tearing modes. However, a proper verification and fuller understanding of the stability of these modes requires a calculation of the linear tearing stability parameter $\Delta'$ for the discharge equilibria, including finite β, strong shaping, and multiple rational surfaces. Improvements in equilibrium diagnostics coupled with improved numerical tools have recently narrowed the ambiguities in tearing stability calculations considerably. Calculations of $\Delta'$ were performed using the PEST-III code [16] for equilibria reconstructed from a low β limiter DIII–D discharge (#97791) at a number of times. The equilibria from the EFIT code were in each case the best fit to the experimental equilibrium data in the sense of minimizing $\chi^2$. The equilibria had $q_0<1$ but β was low enough that no ideal instability was present.

The calculated $\Delta'$ is negative, indicating linear tearing mode stability, until $t \approx 1500$ ms, where it changes sign. At 1550 ms, an m/n=2/1 island begins to grow, as observed from the Mirnov $B_\theta$ signal, consistent with $\Delta'>0$ and a 2/1 instability calculated by PEST-III. However, there is considerable sensitivity of $\Delta'$ to variations in the equilibrium fitting. In particular it was found that if additional constraints, such as forcing $q_0>1$, were imposed, there is then little correlation between the calculated $\Delta'$ and the observed stability. This is in contrast to the case of ideal calculations where $q_0$ is commonly forced above unity [2,17]. It appears that tearing modes are sufficiently sensitive to the changes in the internal profiles so that the procedure of forcing $q_0>1$ does not work.

A more stringent test of the theory and tools is shown in Fig. 6 for a DIII–D high performance discharge #98549 at higher β. In this case, the variety of MHD activity was wider and the calculations were performed for the interesting times near when MHD activity was observed. Again the agreement is remarkably good; the largest positive $\Delta'$ is for the 2/1 mode [Fig. 6(a)] which appears at around 2100 ms. The n=2 amplitude in Fig. 6(c) is mostly from the 4/2 mode which is predicted to be marginally stable linearly but is presumably driven unstable by the 2/1 mode. It is concluded that for this discharge, the MHD modes should be interpreted as classical, linearly unstable tearing modes and not as true NTMs. Sensitivity studies with respect to variations in the equilibrium reconstruction around the minimum $\chi^2$ so far confirm the results and this interpretation. The ability to distinguish between classical tearing and NTM is important for deciding the best strategy for active stabilization.

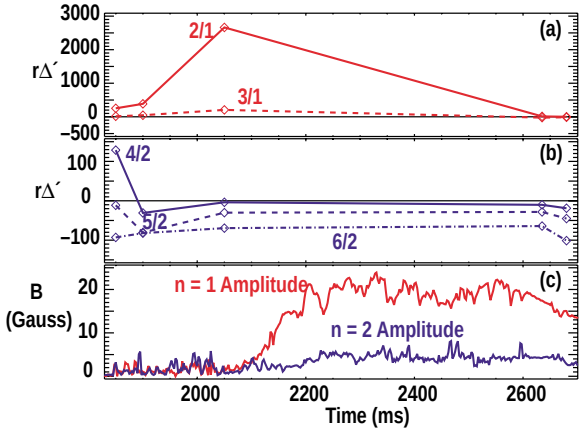


*Fig. 6. $\Delta'$ values for DIII-D high performance discharge#98549 computed from reconstructed equilibria at several times (a) m/n=2/1 and 3/1 modes, (b) m/n=4/2, 5/2, and and 6/2 modes, and (c) observed n=1 and n=2 Mirnov activity.*

However, it should be noted that the increased sensitivity of tearing stability compared to ideal plasma modes (including the RWM) does not always permit an unambiguous result. While considerable progress has been made, as shown here, further refinements in the equilibrium reconstructions are needed to close the gap before the level of agreement between the predictions and observations can approach that of the ideal plasma modes.

## 5. Conclusions

Ideal MHD predictions have advanced well beyond the simple prediction of scaling laws [2] and can now be used to make quantitative predictions of stability limits for specific discharges as well as growth rates and mode structures when these limits are exceeded. The critical improvement spurring this advance is the considerable enhancement in the ability to accurately reconstruct discharge equilibria — especially the MSE measurements of the current profile and high quality pressure profile measurements. Also important, however, is the development of realistic numerical equilibrium reconstruction and stability tools that take account of the measured details in the profiles, cross-section shape, and conducting wall since the results can be quite sensitive to many of these details.

The development of the required numerical tools is still evolving and their continued application to the critical stability issues has already yielded considerable progress in the extension of tokamak discharges toward the advanced tokamak (AT) goal of simultaneous high performance and steady-state. The disruptions that limit highly peaked pressure discharges are now better understood and can be avoided by broadening the pressure profile or controlling the discharge to remain below the predicted $\beta$ limit. A new understanding of edge stability in the presence of steep edge pressure gradients has now been achieved which has provided several avenues to extending the operational limits. Detailed equilibrium reconstructions and ideal stability calculations have been crucial in demonstrating wall stabilization, and identifying the RWM. The computational tools have been extended to simulate active feedback of the RWM and are now important in optimizing the design of the feedback system.

Non-ideal tearing modes are even more sensitive to the profile details than the ideal plasma instabilities. Tools for predicting tearing stability in finite $\beta$, full geometry equilibria with real measured profiles, are now available and can make useful predictions in some cases. Given the remarkable success of ideal MHD in making testable quantitative predictions, continued development and improvements in reconstructing equilibria are likely to result in non-ideal stability codes achieving similar predictive power in the near future. One can then look forward to identifying and isolating competing non-ideal effects and achieving further significant progress toward sustaining stable, long pulse AT discharges.

## Acknowledgments

This is work was supported in part by the U.S. Department of Energy under Grants DE-FG03-95ER54309, DE-FG03-89ER53297, DE-FG02-92ER54139, DE-FG03-95ER54294, Contracts DE-AC03-99ER54463, DE-AC05-75OR00033, DE-AC-2-76CH03073, W-7405-END-36, and by the U.K. Department of Trade and Industry and Euratom.

## References

[1] RICE, B.W., et al., Plasma Phys. **3**, 1983 (1996).
[2] TROYON, F., et al., Plasma Phys. Contr. Fusion **26**, 209 (1984).
[3] CHU, M.S., et al., Phys. Rev. Lett. **77**, 2710 (1996).
[4] TURNBULL, A.D., et al., in Plasma Phys. and Contr. Fusion Res. (1996), Vol. 2, p. 509.
[5] CALLEN, J.D., et al., Phys. Plasmas **6**, 2963 (1999).
[6] STRAIT, E.J., et al., Phys. Plasmas **4**, 1783 (1997).
[7] LAO, L.L., et al., Nucl. Fusion **39**, 1785 (1999).
[8] FERRON, J.R., et al., Phys. Plasmas **7**, 1976 (2000).

[9] GRUBER, R., et al., Compt. Phys. Commun. **24**, 363 (1981).
[10] WILSON, H.R., et al., Phys. Plasmas **6**, 1925 (1999).
[11] TURNBULL, A.D., et al., in Plasma Phys. and Contr. Nucl. Fusion Res. (1994), Vol. I, p. 705.
[12] GAROFALO, A.M., et al., Phys. Rev. Lett. **82**, 3811 (1999).
[13] CHANCE, M.S., et al., this conference.
[14] GAROFALO, A.M., et al., this conference.
[15] LUCE, T.C., et al., this conference.
[16] PLETZER, A., et al., J. Comp. Phys. **115**, 530 (1994).
[17] TURNBULL, A.D., et al., Nucl. Fusion 39, 1557 (1999).